Sense and Shoot: Simultaneous Detection and Degradation of Low-Level Contaminants Using Graphene-Based Smart Material Assembly

Rabeka Alam,[†] Ian V. Lightcap,[†,§] Christopher J. Karwacki,[⊥] and Prashant V. Kamat[†,‡,*]

[†]Radiation Laboratory, [‡]Department of Chemistry & Biochemistry, and [§]Center for Sustainable Energy at Notre Dame, University of Notre Dame, Notre Dame, Indiana 46556, United States and [⊥]Edgewood Chemical Biological Center, U.S. Army Research, Development and Engineering Command, 5183 Blackhawk Road, Aberdeen Proving Ground, Maryland 21010, United States

ABSTRACT *Smart material* nanoassemblies that can simultaneously *sense and shoot* low-level contaminants from air and water are important for overcoming the threat of hazardous chemicals. Graphene oxide (GO) sheets deposited on mesoscopic TiO_2 films that underpin the deposition of Ag nanoparticles with UV irradiation provide the foundation for the design of a smart material. The Ag particle size is readily controlled through precursor concentration and UV irradiation time. These semiconductor–graphene oxide–metal (SGM) films are SERS-active and hence capable of sensing aromatic contaminants such as 4-nitrobenzenethiol (4-NBT) in nanomolar range. Increased local concentration of organic molecules achieved through interaction with 2-D carbon support (GO) facilitates low-level detection of contaminants. Upon UV irradiation of 4-NBT-loaded SGM film, one can induce photocatalytic transformations. Thus, each component of the SGM film plays a pivotal role in aiding the detection and degradation of a contaminant dispersed in aqueous solutions. The advantage of using SGM films as multipurpose "detect and destroy" systems for nitroaromatic molecules is discussed.

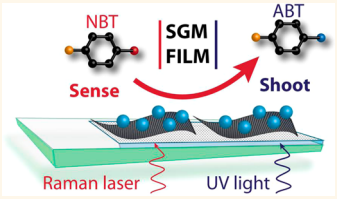

KEYWORDS: graphene oxide · photocatalysis · SERS detection · environmental remediation · nitro compounds · TiO_2

Detection and degradation of trace amounts of hazardous organic compounds in water supplies remain a major challenge. The detection of chemical warfare agents, toxic industrial chemicals, and explosives including nitroaromatics and organophosphonates in water is particularly difficult because they pose a hazard even at low concentrations (ppm–ppb).[1−3] Semiconductor and metal nanostructures offer new opportunities in the construction of chemical sensors as their properties can be tuned with size and shape.[4−10] For example, size-dependent photoluminescence properties of semiconductor nanoparticles (NPs) have been employed for sensing at low concentrations.[9−11] Metal NPs exhibiting localized surface plasmon resonance (LSPR) enhance Raman scattering of organic compounds and thus enable their detection through surface-enhanced Raman spectroscopy (SERS).[7,8,12−15] Several studies offer unsurpassed detection sensitivity, even to the single-molecule level. For example, picomolar concentration of 2,4,6-trinitrotoluene in aqueous solution can be detected using a SERS technique.[7] In addition to superb detection capabilities, metal NPs are also effective in catalyzing the conversion of nitroaromatic compounds to their amino derivatives.[16−18]

While sensing of trace contaminants is of primary importance, the versatility of a device is greatly enhanced if the device can also photocatalytically deactivate the target molecule. Developing a semiconductor–graphene oxide–metal (SGM) system that combines the unique, yet complementary, properties of each component to create a multipurpose device is one way to achieve such functions. With this in mind, each component of the SGM film was carefully selected to serve an exclusive purpose within the larger assembly. Anchoring semiconductor NPs together with metal NPs is a useful approach to improve the functionality of a graphene oxide (GO)-based catalyst mat.[19] For the semiconductor, TiO_2 was selected because it is inexpensive, nontoxic, photostable, and highly effective as

* Address correspondence to pkamat@nd.edu.

Received for review April 29, 2014 and accepted June 3, 2014.

Published online June 03, 2014
10.1021/nn502336x

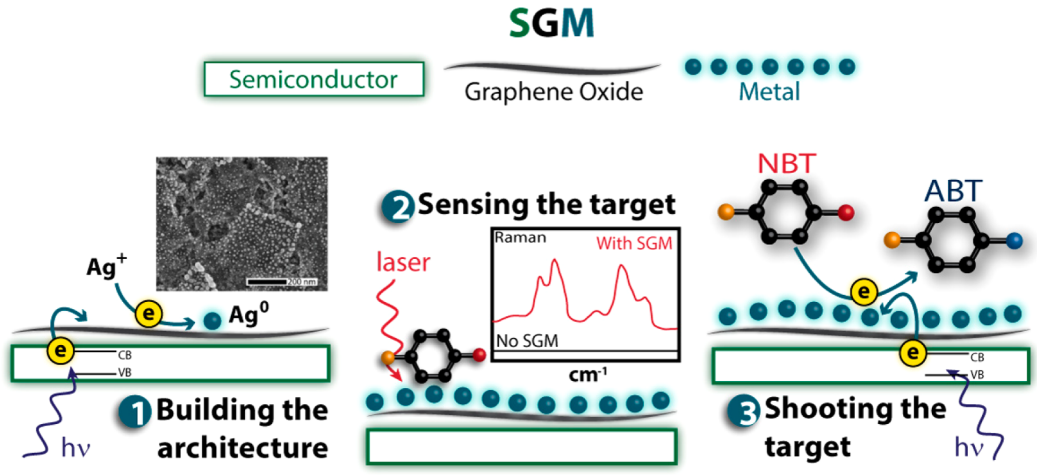

Scheme 1. Combination of semiconductor, graphene oxide, and metal can be leveraged to achieve a *smart material* that can both detect and destroy contaminants. First, the SGM architecture is created by a photoinitiated electron transfer between TiO_2 and GO, which results in the deposition of metal NPs. Second, the GO and metal NPs work in concert to enable detection of trace amounts of the target molecule. Third, another photoinitiated electron transfer, this time from the TiO_2 to the GO to the metal nanoparticles, catalyzes the transformation of the target molecule into a benign form.

a photocatalyst. When TiO_2 undergoes band gap excitation, electron–hole pairs are generated, which can initiate reduction and oxidation of organic compounds in solution.[13] Photocatalytic decomposition of nitro derivatives of organic compounds has already been examined.[20–22] While the semiconductor accomplishes photocatalytic degradation of target molecules, metal NPs are needed to provide a sensing function. Ag NPs were chosen for SGM films for two reasons; first, Ag^+ can be photocatalytically reduced on the TiO_2–GO surface; electrons transferred through GO are energetic enough to reduce silver ions to produce controlled size NPs. Second, Ag NPs show strong SERS enhancement; many studies have shown enhancement by a magnitude of 10^6. The importance of each component in the semiconductor–graphene–metal film is depicted in Scheme 1.

Indeed, the challenge of developing chemical sensors that function both as a detector and decomposer of target molecules can be overcome by combining size-dependent optical and electronic properties of semiconductor and metal NPs. However, it is quite challenging to design uniform semiconductor–hybrid assemblies with desired size in a solution-based approach. For example, it is difficult to control the size and morphology of metal NPs when they are directly grown onto the surface of TiO_2 NPs. Since properties of nanomaterials are dictated by their size and morphology, it is important to be able to control their growth with precision. To overcome these barriers, GO is employed as an intermediate layer to provide a unique 2-D platform to mediate the electronic coupling of semiconductor and metal NPs, while enabling a more consistent and controlled metal deposition.

The ability to mediate electron transport through the 2-D carbon network of GO facilitates communication between semiconductor NPs and metal NPs. Incorporation of single to a few layers of GO facilitates side-segregated growth of NPs, where the metal NPs are deposited mainly on the GO side opposite the semiconductor NPs. Given the ability of carbon substrates to concentrate organic molecules near its surface, and in the case of SGM assemblies, target molecules are brought into close proximity with the metal NPs that can be used for detection.[8,23,24] The ability of GO to accumulate target molecules by adsorption, along with its high surface area, is an additional reason why GO remains an integral component of the SGM film's design sensing function.

RESULTS AND DISCUSSION

In order to utilize the unique electron shuttling properties of reduced graphene oxide (RGO) for growth of Ag NPs, first, GO is electrophoretically deposited (EPD) onto a thin TiO_2 film. EPD of GO onto TiO_2 allows for a controlled deposition of single to a few sheets of GO.[8,23] Once GO is deposited, metal NPs, in particular, Ag NPs, can be readily deposited onto the GO surface through photocatalytic growth. These TiO_2–GO films are activated for metal NP deposition under UV illumination in the presence of metal cations like Ag^+. Equations 1–4 describe the electron transfer process in depositing metal NPs onto TiO_2–GO films. Briefly, upon UV illumination, electrons are photogenerated in TiO_2 and transferred to GO while holes are scavenged by ethanol.[8] The oxidized ethanol (ethoxy radical) also serves as a reducing agent. The electrons are first consumed to form RGO and then shuttled to the opposite side of the RGO, where they reduce Ag^+ ions to Ag^0 NPs. This reaction sequence has the advantage of tuning Ag NP size and overall surface loading of NPs on RGO by regulating the illumination exposure time and metal ion concentration. Furthermore, the favorable nucleation of metal NPs at defect locations such as

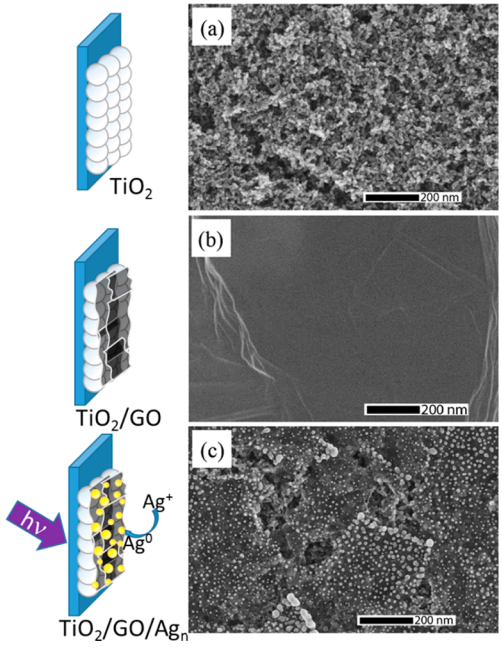

Figure 1. SEM micrographs of (a) TiO_2 NP film, (b) film after electrophoretically depositing single- to few-layer GO over TiO_2, and (c) after photocatalytic deposition of Ag NPs under UV light illumination for 15 min in the presence of 5.9 × 10^{-8} M $AgNO_3$ in ethanol.

epoxide sites on the RGO assist in the metal deposition process.[25−28]

$$TiO_2 + h\nu \rightarrow TiO_2(e + h) \quad (1)$$

$$TiO_2(e + h) + GO \rightarrow TiO_2(h) + RGO(e) \quad (2)$$

$$TiO_2(h) + C_2H_5OH \rightarrow TiO_2 + {}^{\bullet}C_2H_4OH \quad (3)$$

$$RGO_n(e) + nAg^+ \rightarrow RGO + Ag_n \quad (4)$$

This method of depositing metal NPs onto sheets of RGO allows decoupling of direct metal deposition on the semiconductor and avoids formation of irregularly shaped particles with a broad size distribution.[8,19,23] The entire stepwise assembly of the SGM film provides a simple yet robust method for controlling size and morphology of metal NPs on a 2-D substrate. Figures 1a and b show scanning electron microscopy (SEM) images of TiO_2 films before and after GO deposition. The mesoscopic TiO_2 film covered with one to few layers of GO sheets exhibits distinctly visible wrinkles. Introducing Ag^+ ions to the TiO_2−GO films and subjecting the film to illumination of UV light results in the formation of Ag NPs and, thus, the completion of the SGM film framework. Figure 1c shows the SGM film surface decorated with Ag NPs. A large density of Ag NPs covered throughout the surface of RGO sheet is noticeable with deposition preference at edge sites.

An interesting aspect of the stepwise construction of SGM assembly is the ability to control Ag NP size with UV illumination time or the concentration of Ag^+ ions in solution. Figure 2 shows representative SEM images of SGM films with different sizes of Ag NPs of 12−40 nm diameter range obtained through concentration variation (histograms showing size distribution of particle size is provided in Supporting Information Figure S2). The concentration of $AgNO_3$ in ethanol solution was varied between 5.9 × 10^{-8} and 4.7 × 10^{-7} M, and the TiO_2 film was subjected to a constant period of UV illumination (1.6 W/cm^2, illumination time 15 min) (detailed experimental protocol is provided in the Supporting Information). The metal NP arrays deposited on RGO sheets exhibit a narrow size distribution with high levels of loading. For Ag NPs of 40 nm diameter or larger, a seeded method provides a better control for maintaining the particle growth. In this approach, the small Ag NPs are first grown onto RGO, and then they are further ripened *via* slow addition of small aliquots of Ag^+ ions to the solution. By constructing these SGM architectures with different sizes of Ag NPs, it is possible to probe the metal NP size effect on SERS activity.

SERS is a valuable tool for the detection of trace molecules; it utilizes the interaction between the target molecule and the LSPR of noble metal NPs, like Ag, to amplify the Raman signal of the target molecule. Additionally, the RGO in SGM films can enhance SERS signals due to fluorescence quenching along with its Raman-enhancing properties.[8,23] Here, we explored the ability of these SGM films to act as chemical sensors by employing 4-nitrobenzenethiol (4-NBT) as the target molecule. SGM films were placed in 1.0 mL of ethanol solution of submicromolar concentrations of 4-NBT, and SERS experiments were carried out in a cuvette with a 5 mm path length using 514 nm laser excitation source.

Figure 3a shows representative absorption spectra of SGM films prepared with different Ag NPs. The absorbance corresponding to Ag surface plasmon is observed in the 400−500 nm region. Because of the broad nature of the plasmon peak, we could not analyze its dependence on the particle size. Figure 3b shows SERS spectra recorded with the SGM film in contact with 1 mL of 500 nM 4-NBT in ethanol. The spectra were recorded after subtracting the Raman signal of SGM in ethanol without any target molecules. Control experiments carried out with 4-NBT in ethanol and with TiO_2−GO film show no detectable Raman signal. However, SGM films under the same conditions exhibit significant enhancement of the Raman signal of 4-NBT as Ag NPs deposited on RGO serve as SERS-active sites. SGM films with larger size Ag NPs exhibit greater sensitivity. The prominent peak around 1340 cm^{-1} is indicative of the symmetric stretching vibration of the nitro group [$\nu_s(NO_2)$],[29,30] the intensity of which prominently increased with increasing Ag particle size. Additionally, a band around 1560 cm^{-1} corresponding to the asymmetric stretching vibration

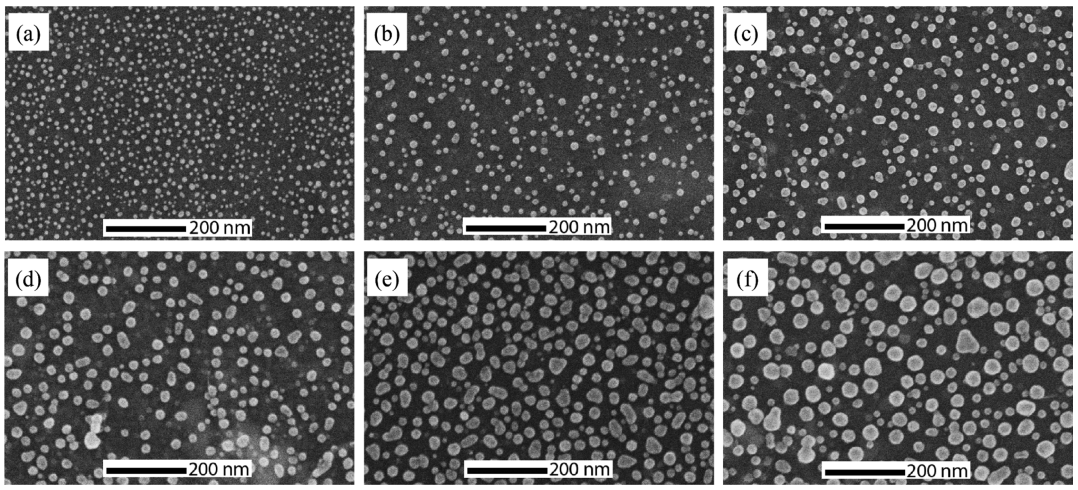

Figure 2. SEM micrographs of SGM films with varying Ag NP size: (a) $d = 12.8 \pm 3.5$ nm (SGM(1)); (b) $d = 16.6 \pm 3.1$ nm (SGM(2)); (c) $d = 22.3 \pm 4.4$ nm (SGM(3)); (d) $d = 28.8 \pm 3.9$ nm (SGM(4)); (e) $d = 30.0 \pm 6.7$ nm (SGM(5)); (f) $d = 40.8 \pm 5.1$ nm (SGM(6)). Ag NP size is controlled by changing $AgNO_3$ concentration; 15 min deposition time used for samples a−e, 30 min used for SMG(6) (f). Size distributions of NPs are based on analysis of 100 NPs on ImageJ software.

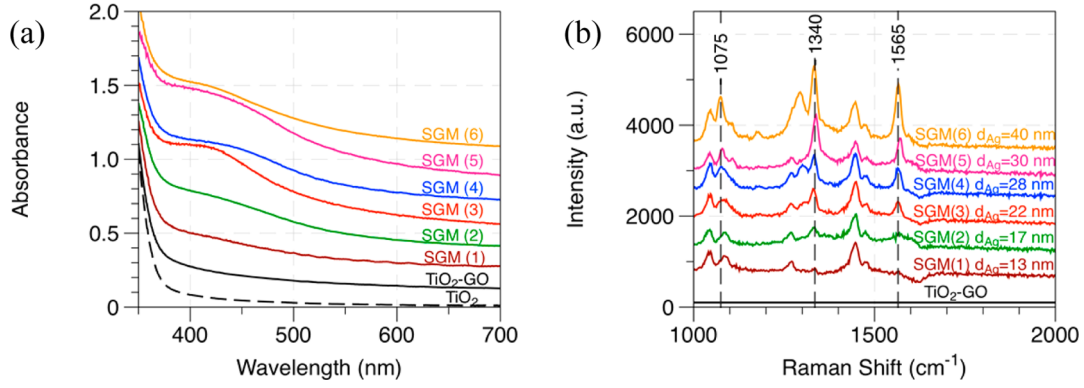

Figure 3. (a) Representative UV−visible absorption spectra of SGM films with varying Ag NP size. Deposition of larger Ag NP sizes causes increased surface plasmon absorption in SGM films, seen between 400 and 500 nm. (b) SERS spectra of 500 nM 4-NBT in ethanol in the presence of SGM films. All films were placed in 1 mL of 500 nM 4-NBT in ethanol and allowed to sit for 30 min prior to SERS measurements. Raman signal from SGM and ethanol has been subtracted from SERS spectra. Increase in SERS signal is observed with increasing Ag NP size, in particular, an increase is observed for $[\nu_s(NO_2)]$ at 1340 cm^{-1}. All SGM films were prepared with an active surface area of 0.16 cm^2. Both absorption and SERS data baselines have been offset manually for clarity.

of $[\nu_a(NO_2)]$ and stretching vibration $[\nu(C-S)]$ at 1075 cm^{-1} are also seen.

SGM film sensors permit the flexibility of sensing a wide range of molecules since RGO can concentrate a low level of organic molecules from solution onto the RGO and in the close proximity of deposited metal NP interface. One such example of $\pi-\pi$ interaction between RGO film and porphyrin molecules has been discussed in an earlier study.[31] Thus, SGM architectures provide a versatile platform for detection of a broad range of molecules at low concentration levels. For example, the SERS response of SGM film to varying concentration of 4-NBT is shown in Figure 4.

RGO not only provides a unique 2-D platform for the building of a strip-based sensor but also facilitates adsorption of the organic molecules, thus increasing the local chemical concentration. In addition to sp^2 regions, the surface of RGO is decorated with epoxy,

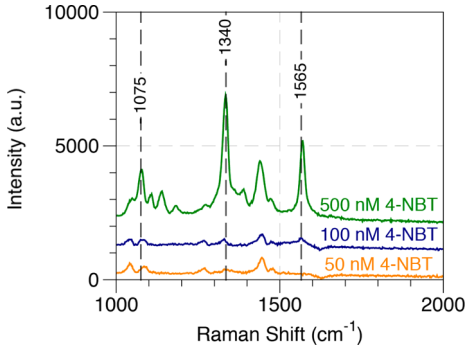

Figure 4. SERS spectra of 4-NBT in the presence of SGM film (average Ag NP size 30 nm) with an active area of 0.16 cm^2 at 4-NBT concentrations of 50, 100, and 500 nM in ethanol. Films were soaked for 30 min before collecting SERS spectra. Data have been offset manually in the graph.

hydroxyl, and carboxylic acid functional groups that are found to enhance interactions with target

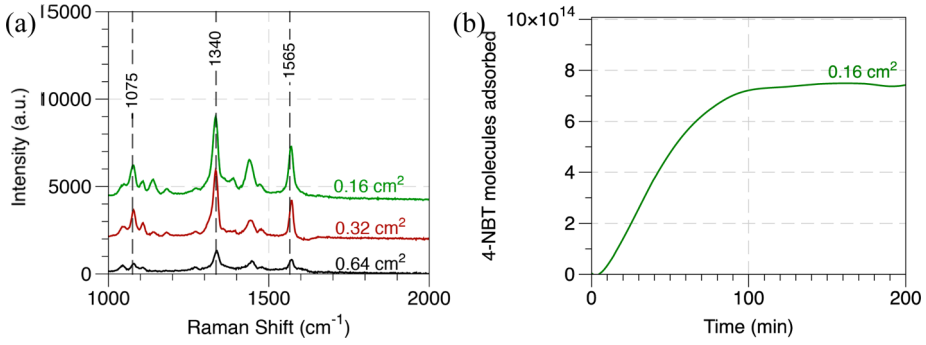

Figure 5. (a) SERS spectra of 4-NBT on SGM films with different size active area: 0.16, 0.32, and 0.64 cm^2. SGM films with an average Ag NP size of 30 nm were soaked in 1 mL of 500 nM 4-NBT in ethanol for 24 h before collecting SERS data. Increase in intensity of symmetric vibration stretching of NO_2 at 1340 cm^{-1} is observed with decreasing active area, due to a greater number of target molecules available per cm^2. SERS data have been baseline-corrected for clarity. (b) 4-NBT adsorption (expressed in terms of molecules adsorbed) onto SGM films with 0.16 cm^2 active area sizes over 200 min. Saturation of molecules adsorbed onto SGM films is reached by 100 min.

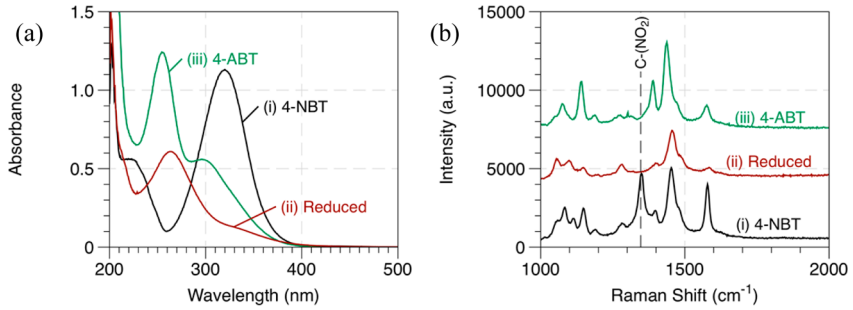

Figure 6. (a) UV−vis absorption and (b) SERS spectra showing photocatalytic reduction of 4-NBT to 4-ABT in ethanol. The spectra were recorded before (i) and after (ii) UV irradiation of SGM film for 15 min. Spectrum (iii) shows reference sample of 4-ABT in ethanol. Absorption spectra were collected using 10 μM 4-NBT (or 4-ABT) in ethanol in a 1 cm cuvette. SERS experiment was performed with 500 nM 4-NBT (or 4-ABT) in ethanol.

molecules due to dipole−dipole attractions.[32−34] It has also been reported that organic species interact with graphene oxide through van der Waals forces, which further assists in the concentration of target molecules onto the RGO surface.[31,34] These interactions act as anchors to attract and immobilize molecules at the film interface.

The proposed concentrating effect of RGO for chemical sensing was probed as a function of geometric RGO surface area (active area), as shown in Figure 5a. SGM films were prepared with active areas of 0.16 cm^2 (0.4 cm × 0.4 cm), 0.32 cm^2 (0.8 cm × 0.4 cm), and 0.64 cm^2 (1.6 cm × 0.4 cm) then soaked in 500 nM 4-NBT in ethanol solution for 24 h before collecting SERS spectra. Interestingly, films with the smallest active area (0.16 cm^2) showed the most intense Raman signal, as the smaller area is more likely to have adsorbed target molecules in the limited area probed by the Raman laser. This observation further supports the argument that the SERS response corresponds to adsorbed molecules on the GO surface and is not being collected from the molecules in solution. The correlation of SERS signal enhancement with decreasing active area points to the concentrating effect of GO. Adsorption of 4-NBT onto SGM films was also monitored by measuring the decrease in absorbance of free 4-NBT in solution over time, which can then be correlated to the number of 4-NBT molecules adsorbed onto SGM films. Figure 5b shows number of 4-NBT molecules adsorbed to SGM film of 0.16 cm^2 active area over a period 200 min (additional adsorption data are shown in Figure S3). After exposing SGM films to 500 nM 4-NBT solutions for 100 min, equilibrium is reached. This study provided further evidence that target molecules interact with the graphene surface.

In addition to sensing low levels of nitroaromatics, it is also crucial to attain simple ways to destroy them. Reduction of 4-NBT is accomplished by irradiating SGM films with UV light for 15 min, a process that results in electron transfer from SGM film to 4-NBT, facilitating the reduction of the nitro functional group to form 4-aminobenzenethiol (4-ABT) (reactions 2 and 5).

$$\mathrm{RGO}(e) + \text{4-NBT} + \mathrm{H^+}(\mathrm{H_2O}) \rightarrow \mathrm{RGO} + \text{4-ABT} \quad (5)$$

Figure 6a shows the absorption spectra of 4-NBT and 4-ABT standard solutions and 4-NBT solution after reduction of the nitro functional group to an amino group following UV irradiation of the SGM film. After irradiating 4-NBT with UV light, the characteristic absorption peak at 320 nm disappears and a peak at 256 nm begins to appear that is characteristic of 4-ABT. The reduction of 4-NBT to 4-ABT can also be probed

through SERS measurements. The complete disappearance of a characteristic [$\nu_s(NO_2)$] peak around 1340 cm^{-1} seen after irradiation with UV light confirms the transformation of 4-NBT (Figure 6b).

CONCLUSIONS

In summary, single to few layers of GO deposited on mesoscopic semiconductor film provides a 2-D network that is photocatalytically active for deposition of Ag NPs with tailored NP size and surface coverage, achieved *via* metal ion concentration and illumination time during deposition. Combining the ability of RGO to concentrate target molecules with SERS-active and catalytic Ag NPs provides a robust foundation for multipurpose sense and destroy applications. SGM films prepared using this versatile technique can be adapted to fit a wide range of sensing and photocatalytic applications. The example discussed above shows the effectiveness of SGM film as a photocatalyst and assists in the transformation of an organic pollutant to a less toxic compound. Efforts are underway to extend this degradation strategy to aqueous systems and carry out complete mineralization of hazardous chemicals by making use of TiO_2-induced photocatalysis.

MATERIALS AND METHODS

Preparation of TiO_2–GO Films. TiO_2 (d = ~15–20 nm) paste (Solaronix, Ti-nanoxide T/SP) was applied to the conducting side of optically transparent electrode (OTE) *via* the doctor blade method. The TiO_2–OTE films were annealed at 80 °C for 30 min, followed by 1 h at 500 °C. Before deposition of GO onto TiO_2, the GO suspension in ethanol was sonicated for 1 h and allowed to settle for several hours to overnight. This long period of sedimentation allows for stacked GO to fall out of solution, leaving a more single-layer GO in solution. Electrophoretic deposition of single-layer GO onto TiO_2 involves submersion of TiO_2 films into 2.5 mL of ~0.3 mg/mL GO dispersion. A counter electrode was held parallel to the TiO_2 film at a distance of 4 mm, with the conducting sides of the two electrodes facing one another. A voltage of 60 V was applied between the two OTEs, and deposition was carried out for 45 s.

Deposition of Metal Nanoparticles onto TiO_2–GO Film. Prepared TiO_2–GO films were submerged in ethanol (10 mL) and purged with N_2 for 15 min. For deposition of Ag NPs, $AgNO_3$ in ethanol was used. For the light-induced growth of metal NPs, the film was placed ~35 cm from a 300 W Xe lamp (Oriel) and back side illuminated for time intervals ranging between 15 min. The concentration of $AgNO_3$ was adjusted between 5.9×10^{-8} and 4.7×10^{-7} M to grow Ag NPs of different sizes.

Optical and Structural Characterization of SGM Films. Optical absorption spectra were collected on a Varian Cary 50 Bio UV–visible spectrometer. Morphology and size of SGM were examined using FEI Magellan-400 field emission scanning electron microscope.

Surface-Enhanced Resonance Raman Spectroscopy and Fourier Transform Infrared Spectroscopy. The Raman signal enhancement was analyzed using a Renishaw Raman microscope (RM1000) equipped with a 514 nm argon ion laser excitation source. SGM films were immersed in ethanol with nanomolar concentration of the target molecule and placed front side, with respect to incident laser, in a sealed 5 mm optical cuvette. FTIR spectra were collected in a Shimadzu FTIR-8400S spectrometer.

Conflict of Interest: The authors declare no competing financial interest.

Acknowledgment. The research described in this paper is supported by the Army Research Office through the award ARO 64011-CH. This is a document number 5022 from the Notre Dame Radiation Laboratory, which is supported by the Division of Chemical Sciences, Geosciences, and Biosciences, Office of Basic Energy Sciences of the U.S. Department of Energy through award DE-FC02-04ER15533.

Supporting Information Available: Synthesis and characterization of graphene oxide, histograms of silver nanoparticle distribution, and adsorption isotherms are included. This material is available free of charge *via* the Internet at http://pubs.acs.org.

REFERENCES AND NOTES

1. Lewis, T. A.; Newcombe, D. A.; Crawford, R. L. Bioremediation of Soils Contaminated with Explosives. *J. Environ. Manage.* **2004**, *70*, 291–307.
2. Lynch, J. C.; Brannon, J. M.; Delfino, J. J. Dissolution Rates of Three High Explosive Compounds: TNT, RDX, and HMX. *Chemosphere* **2002**, *47*, 725–734.
3. Letzel, S.; Goen, T.; Bader, M.; Angerer, J.; Kraus, T. Exposure to Nitroaromatic Explosives and Health Effects during Disposal of Military Waste. *Occup. Environ. Med.* **2003**, *60*, 483–488.
4. Germanenko, I. N.; Li, S. T.; El-Shall, M. S. Decay Dynamics and Quenching of Photoluminescence from Silicon Nanocrystals by Aromatic Nitro Compounds. *J. Phys. Chem. B* **2001**, *105*, 59–66.
5. Sohn, H.; Letant, S.; Sailor M, J.; Trogler, W. C. Detection of Fluorophosphonate Chemical Warfare Agents by Catalytic Hydrolysis with a Porous Silicon Interferometer. *J. Am. Chem. Soc.* **2000**, *122*, 5399–5400.
6. Jain, P. K.; Huang, X.; El-Sayed, I. H.; El-Sayed, M. A. Noble Metals on the Nanoscale: Optical and Photothermal Properties and Some Applications in Imaging, Sensing, Biology, and Medicine. *Acc. Chem. Res.* **2008**, *41*, 1578–1586.
7. Dasary, S. S. R.; Singh, A. K.; Senapati, D.; Yu, H.; Ray, P. C. Gold Nanoparticle Based Label-Free SERS Probe for Ultrasensitive and Selective Detection of Trinitrotoluene. *J. Am. Chem. Soc.* **2009**, *131*, 13806–13812.
8. Lightcap, I. V.; Murphy, S.; Schumer, T.; Kamat, P. V. Electron Hopping through Single-to-Few Layer Graphene Oxide Films. Photocatalytically Activated Metal Nanoparticle Deposition. *J. Phys. Chem. Lett.* **2012**, *3*, 1453–1458.
9. Freeman, R.; Finder, T.; Bahshi, L.; Gill, R.; Willner, I. Functionalized CdSe/ZnS QDs for the Detection of Nitroaromatic or RDX Explosives. *Adv. Mater.* **2012**, *24*, 6416–6421.
10. Zhang, K.; Mei, Q.; Guan, G.; Liu, B.; Wang, S.; Zhang, Z. Ligand Replacement-Induced Fluorescence Switch of Quantum Dots for Ultrasensitive Detection of Organophosphorothioate Pesticides. *Anal. Chem.* **2010**, *82*, 9579–9586.
11. Medintz, I. L.; Uyeda, H. T.; Goldman, E. R.; Mattoussi, H. Quantum Dot Bioconjugates for Imaging, Labelling and Sensing. *Nat. Mater.* **2005**, *4*, 435–446.
12. Blaber, M. G.; Henry, A.-I.; Bingham, J. M.; Schatz, G. C.; Van Duyne, R. P. LSPR Imaging of Silver Triangular Nanoprisms: Correlating Scattering with Structure Using Electrodynamics for Plasmon Lifetime Analysis. *J. Phys. Chem. C* **2012**, *116*, 393–403.
13. Kamat, P. V.; Meisel, D. Nanoparticles in Advanced Oxidation Processes. *Curr. Opin. Colloid Interface Sci.* **2002**, *7*, 282–287.
14. Lopez-Puente, V.; Abalde-Cela, S.; Angelome, P. C.; Alvarez-Puebla, R. A.; Liz-Marzan, L. M. Plasmonic Mesoporous Composites as Molecular Sieves for SERS Detection. *J. Phys. Chem. Lett.* **2013**, *4*, 2715–2720.

15. Grzelczak, M.; Liz-Marzan, L. M. Colloidal Nanoplasmonics: From Building Blocks to Sensing Devices. *Langmuir* **2013**, *29*, 4652–4663.
16. Shin, K. S.; Lee, S. W.; Han, K. C.; Kim, S. K.; Yang, E. K.; Park, J. H.; Ju, B. K.; Kang, J. Y.; Kim, T. S. Amplification of Fluorescence with Packed Beads To Enhance the Sensitivity of Miniaturized Detection in Microfluidic Chip. *Biosens. Bioelectron.* **2007**, *22*, 2261–2267.
17. Xia, Y.; Song, L.; Zhu, C. Turn-On and Near-Infrared Fluorescent Sensing for 2,4,6-Trinitrotoluene Based on Hybrid (Gold Nanorod)−(Quantum Dots) Assembly. *Anal. Chem.* **2011**, *83*, 1401–1407.
18. Lou, X. B.; He, L.; Qian, Y.; Liu, Y. M.; Cao, Y.; Fan, K. N. Highly Chemo- and Regioselective Transfer Reduction of Aromatic Nitro Compounds Using Ammonium Formate Catalyzed by Supported Gold Nanoparticles. *Adv. Synth. Catal.* **2011**, *353*, 281–286.
19. Krishnamurthy, S.; Kamat, P. V. Galvanic Exchange on Reduced Graphene Oxide. Designing a Multifunctional Two-Dimensional Catalyst Assembly. *J. Phys. Chem. C* **2013**, *117*, 571–577.
20. Peller, J.; Wiest, O.; Kamat, P. V. Hydroxyl Radical's Role in the Remediation of a Common Herbicide, 2,4-Dichlorophenoxyacetic acid (2,4-D). *J. Phys. Chem. A* **2004**, *108*, 10925–10933.
21. Schmelling, D.; Gray, K. A. Photocatalytic Transformation of 2,4,6 Trinitrotoluene. *Water Res.* **1995**, *29*, 2651.
22. Cropek, D.; Kemme, P. A.; Makarova, O. V.; Chen, L. X.; Rajh, T. Selective Photocatalytic Decomposition of Nitrobenzene Using Surface Modified TiO_2 Nanoparticles. *J. Phys. Chem. C* **2008**, *112*, 8311–8318.
23. Lightcap, I. V.; Kamat, P. V. Graphitic Design: Prospects of Graphene-Based Nanocomposites for Solar Energy Conversion, Storage, and Sensing. *Acc. Chem. Res.* **2013**, *46*, 2235–2243.
24. Fan, Z.; Kanchanapally, R.; Ray, P. C. Hybrid Graphene Oxide Based Ultrasensitive SERS Probe for Label-Free Biosensing. *J. Phys. Chem. Lett.* **2013**, *4*, 3813–3818.
25. Goncalves, G.; Marques, P. A. A. P.; Granadeiro, C. M.; Nogueira, H. I. S.; Singh, M. K.; Gracio, J. Surface Modification of Graphene Nanosheets with Gold Nanoparticles: The Role of Oxygen Moieties at Graphene Surface on Gold Nucleation and Growth. *Chem. Mater.* **2009**, *21*, 4796–4802.
26. Lazar, P.; Zhang, S.; Safarova, K.; Li, Q.; Froning, J. P.; Granatier, J.; Hobza, P.; Zboril, R.; Besenbacher, F.; Dong, M.; Otyepka, M. Quantification of the Interaction Forces between Metals and Graphene by Quantum Chemical Calculations and Dynamic Force Measurements under Ambient Conditions. *ACS Nano* **2013**, *7*, 1646–1651.
27. Wang, M. X.; Liu, Q.; Li, Z. F.; Sun, H. F.; Stach, E. A.; Xie, J. Structural Modification of Graphene Sheets To Create a Dense Network of Defect Sites. *J. Phys. Chem. Lett.* **2013**, *4*, 1484–1488.
28. Zan, R.; Bangert, U.; Ramasse, Q.; Novoselov, K. S. Interaction of Metals with Suspended Graphene Observed by Transmission Electron Microscopy. *J. Phys. Chem. Lett.* **2012**, *3*, 953–958.
29. Kelly, K. L.; Coronado, E.; Zhao, L. L.; Schatz, G. C. The Optical Properties of Metal Nanoparticles: The Influence of Size, Shape, and Dielectric Environment. *J. Phys. Chem. B* **2003**, *107*, 668–677.
30. Stamplecoskie, K. G.; Scaiano, J. C.; Tiwari, V. S.; Anis, H. Optimal Size of Silver Nanoparticles for Surface-Enhanced Raman Spectroscopy. *J. Phys. Chem. C* **2011**, *115*, 1403–1409.
31. Wojcik, A.; Kamat, P. V. Reduced Graphene Oxide and Porphyrin. An Interactive Affair in 2-D. *ACS Nano* **2010**, *4*, 6697–6706.
32. He, H. Y.; Klinowski, J.; Forster, M.; Lerf, A. A New Structural Model for Graphite Oxide. *Chem. Phys. Lett.* **1998**, *287*, 53–56.
33. Lopes, M.; Candini, A.; Urdampilleta, M.; Reserbat-Plantey, A.; Bellini, V.; Klyatskaya, S.; Marty, L.; Ruben, M.; Affronte, M.; Wernsdorfer, W.; Bendiab, N. Surface-Enhanced Raman Signal for Terbium Single-Molecule Magnets Grafted on Graphene. *ACS Nano* **2010**, *4*, 7531–7537.
34. Jung, N.; Crowther, A. C.; Kim, N.; Kim, P.; Brus, L. Raman Enhancement on Graphene: Adsorbed and Intercalated Molecular Species. *ACS Nano* **2010**, *4*, 7005–7013.